THE JOURNAL OF BIOLOGICAL CHEMISTRY VOL. 291, NO. 37, pp. 19437–19448, Septemer 9, 2016
© 2016 by The American Society for Biochemistry and Molecular Biology, Inc. Published in the U.S.A.

Quantification of the Relative Contributions of Loss-of-function and Gain-of-function Mechanisms in TAR DNA-binding Protein 43 (TDP-43) Proteinopathies*[S]

Received for publication, May 11, 2016, and in revised form, July 12, 2016 Published, JBC Papers in Press, July 21, 2016, DOI 10.1074/jbc.M116.737726

Roberta Cascella[‡], **Claudia Capitini**[‡], **Giulia Fani**[‡], **Christopher M. Dobson**[§], **Cristina Cecchi**[‡], **and Fabrizio Chiti**[‡1]

From the [‡]*Section of Biochemistry, Department of Experimental and Clinical Biomedical Sciences, University of Florence, V.le GB Morgagni 50, 50134 Florence, Italy and* [§]*Department of Chemistry, University of Cambridge, Lensfield Road, Cambridge, CB2 1EW United Kingdom*

Amyotrophic lateral sclerosis (ALS) and frontotemporal lobar degeneration with ubiquitin positive inclusions (FTLD-U) are two clinically distinct neurodegenerative conditions sharing a similar histopathology characterized by the nuclear clearance of TDP-43 and its associated deposition into cytoplasmic inclusions in different areas of the central nervous system. Given the concomitant occurrence of TDP-43 nuclear depletion and cytoplasmic accumulation, it has been proposed that TDP-43 proteinopathies originate from either a loss-of-function (LOF) mechanism, a gain-of-function (GOF) process, or both. We have addressed this issue by transfecting murine NSC34 and N2a cells with siRNA for endogenous murine TDP-43 and with human recombinant TDP-43 inclusion bodies (IBs). These two strategies allowed the depletion of nuclear TDP-43 and the accumulation of cytoplasmic TDP-43 aggregates to occur separately and independently. Endogenous and exogenous TDP-43 were monitored and quantified using both immunofluorescence and Western blotting analysis, and nuclear functional TDP-43 was measured by monitoring the sortilin 1 mRNA splicing activity. Various degrees of TDP-43 cytoplasmic accumulation and nuclear TDP-43 depletion were achieved and the resulting cellular viability was evaluated, leading to a quantitative global analysis on the relative effects of LOF and GOF on the overall cytotoxicity. These were found to be ~55% and 45%, respectively, in both cell lines and using both readouts of cell toxicity, showing that these two mechanisms are likely to contribute apparently equally to the pathologies of ALS and FTLD-U.

Amyotrophic lateral sclerosis (ALS)[2] and frontotemporal lobar degeneration with ubiquitin positive inclusions (FTLD-U) are neurodegenerative conditions with distinct clinical profiles but sharing a similar histopathology characterized by the cytoplasmic deposition of proteinaceous inclusions of the TAR DNA-binding protein 43 (TDP-43) in different regions of the central nervous system (1, 2).

From a clinical viewpoint, ALS is characterized by progressive muscle weakness, atrophy, fasciculation, spasticity, difficulty in moving, speaking, swallowing, and breathing, with all these symptoms reflecting progressive degeneration of motoneurons of the primary motor cortex, corticospinal tracts, brainstem, and spinal cord (3, 4). TDP-43 inclusion formation involves the cytosol of upper and lower motoneurons of the brain, brainstem, and spinal cord in all patients, and of neurons of the frontotemporal cortex and hippocampus in a subset of cases (1, 2). Inclusion bodies of TDP-43 were also found in the glial cells of the brainstem and spinal cord of ALS patients (2).

FTLD is a form of cortical dementia involving degeneration of the frontal and temporal lobes of the brain (5). It is characterized either by changes in personality and behavior or by language dysfunction (aphasia). In neuropathological terms, FTLD can be divided in three forms: FTLD with tau-positive inclusions, FTLD with tau-negative, ubiquitin-positive, and TDP-43-positive inclusions (FTLD-U or FTLD-TDP), and FTLD with ubiquitin-positive inclusions that are also positive for the fused in sarcoma protein (FTLD-FUS). In FTLD-TDP the inclusions are mainly cytoplasmic and are present in the frontal and temporal cortices, hippocampus, with the frequent involvement of brainstem and spinal cord motor neurons (1).

In both ALS and FTLD-U the formation of cytoplasmic TDP-43 inclusions in neurons and motoneurons is accompanied by post-translational modifications of the TDP-43 protein (1). These modifications include N-terminal truncation, to generate a mixture of full-length protein and C-terminal fragments, hyperphosphorylation and ubiquitination. In addition, the accumulation of TDP-43 in the cytoplasm occurs concomitantly with its depletion from the nucleus, where TDP-43 normally resides in its soluble and functional form. Given the concomitant occurrence of TDP-43 nuclear depletion and cytoplasmic accumulation, it has been proposed that TDP-43 proteinopathies originate either from a loss-of-function (LOF) mechanism, resulting from a decrease of functional TDP-43 levels in the nucleus, a gain-of-function (GOF) mechanism, resulting from the formation of potentially harmful TDP-43 cytoplasmic inclusions, or a combination of the two mechanisms (6–11). If both mechanisms are at work, as many investigators suppose, it has not yet been established which of the two is the most prominent contributor to the disease pathology.

* This work was supported by the Fondazione Cassa di Risparmio di Pistoia e Pescia (Project no. 2014.0251). The authors declare that they have no conflicts of interest with the contents of this article.

[S] This article contains supplemental Figs. S1–S7 and methods.

[1] To whom correspondence should be addressed. E-mail: fabrizio.chiti@unifi.it.

[2] The abbreviations used are: ALS, amyotrophic lateral sclerosis; FTLD-U, frontotemporal lobar degeneration with ubiquitin positive inclusions; GOF, gain-of-function; IB, inclusion body; LOF, loss-of-function; Sort1, mouse sortilin 1; siRNA, small-interfering RNA; TDP-43, TAR DNA-binding protein 43; MTT, 3,(4,5-dimethylthiazol-2)2,5 diphenyltetrazolium bromide.

This is an Open Access article under the CC BY license.

Studies in mammalian cell cultures and animal models have not clarified this issue. In cultured mammalian cells, for example, overexpression of full-length TDP-43 generally results in a nuclear enrichment of TDP-43 in the absence of cytosolic mislocalization (12–20), and in no, or only low, levels of cellular damage (15, 17–20). Expression of C-terminal fragments of the protein (Ct TDP-43) or of protein lacking the nuclear localization signal (ΔNLS TDP-43), has resulted in cytoplasmic inclusion formation and nuclear depletion, with the cytoplasmic inclusions found to recruit nuclear TDP-43 (12–16, 20). Translocation of TDP-43 from the nucleus to the cytoplasm has been found to result in marked toxicity (15, 20), but it has been difficult to induce nuclear clearance and inclusion formation separately. Importantly, knockdown experiments of TDP-43 in Neuro2a cells were found to inhibit neurite growth, diminish cell viability, and induce apoptosis, indicating that loss of functional nuclear TDP-43 is intrinsically deleterious (13, 21).

Overexpression of full-length TDP-43 in transgenic mice has resulted in neuronal loss and phenotypic abnormalities in part reminiscent of ALS and FTLD in a clear dose-dependent manner (22–28). In these animals, TDP-43 overexpression has often led to enrichment of TDP-43 in the nucleus in the absence of significant formation of cytoplasmic inclusions, thereby indicating that an increase in nuclear TDP-43 levels is sufficient to trigger neurodegeneration (22–28). In a few cases where inclusions form in combination with nuclear depletion, however, the phenotypic abnormalities have appeared to be more severe (23, 24, 26, 28, 29), suggesting that both events could contribute to cellular damage. As in the cell culture experiments, however, it has been difficult to induce nuclear clearance and cytosolic accumulation separately and hence to evaluate their individual contributions to the observed toxicity. Importantly, complete loss of TDP-43 in murine knock-out experiments have resulted in early embryonic lethality, implying that the presence of functional nuclear TDP-43 is essential for life (30–32).

In the light of all these studies, it is clear that the major problem in establishing a fundamental distinction between LOF and GOF mechanisms in ALS and FTLD-U originates from the simultaneous occurrence of nuclear depletion and cytoplasmic accumulation of TDP-43 in human patients, as well as in their related animal and cell culture models. In addition, overexpression of TDP-43 in cell cultures or transgenic animals often results in enrichment of TDP-43 in the nucleus and toxicity, in the absence of any significant mislocalization of the protein, complicating still further the elucidation of this issue. In this paper we have utilized a combined approach to dissect TDP-43 nuclear depletion and cytosolic accumulation of TDP-43 in cells. We have first transiently overexpressed human TDP-43 to different degrees and reproduced previous findings of nuclear enrichment at normally used levels of expression and nucleus-to-cytosol mislocalization at very high expression levels. We have then used RNA interference and internalization of preformed inclusion bodies containing TDP-43, with the aim of causing nuclear depletion of TDP-43 in the absence of mislocalization, and accumulation of cytosolic TDP-43 aggregates in the absence of nuclear alterations, respectively. This approach has allowed us to evaluate the GOF and LOF contributions to cytotoxicity separately and to quantify their relative roles in the overall toxicity caused by the aberrant behavior of TDP-43.

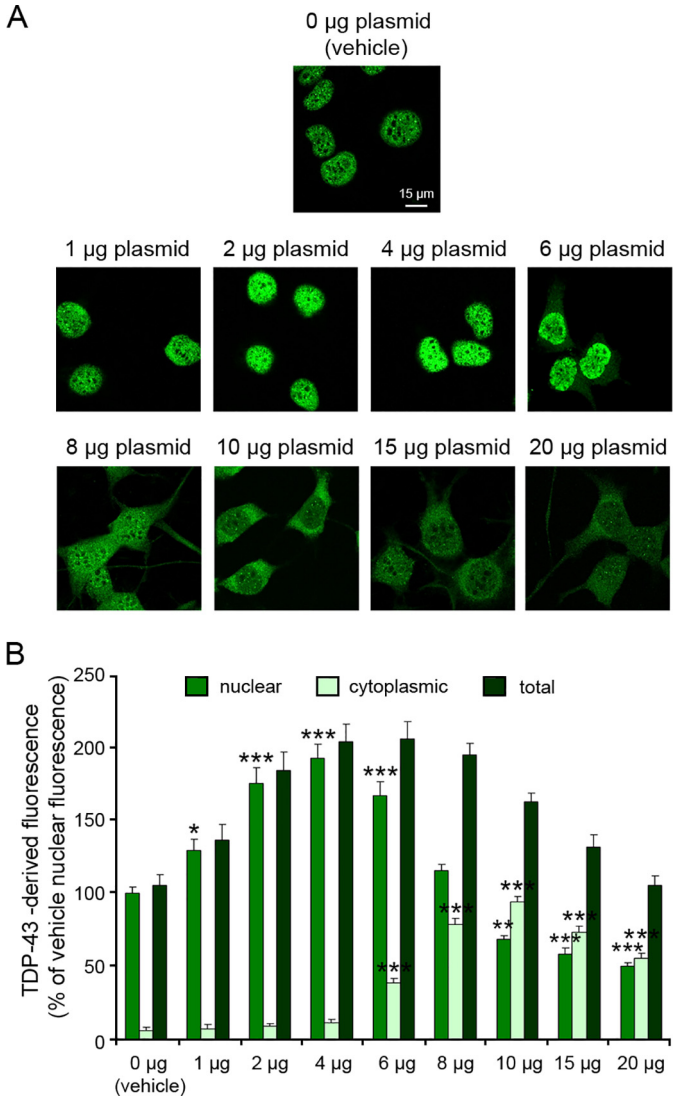

FIGURE 1. *A*, representative confocal scanning microscope images of murine NSC34 cells transiently transfected with different quantities (0–20 μg) of pCI-neo plasmid expressing human TDP-43 and acquired after 48 h. The green fluorescence indicates TDP-43 detected with antibodies that recognize both the endogenous (murine) and exogenous (human) protein. *B*, semi-quantitative analysis of nuclear (*green*), cytoplasmic (*pale green*) and total (*dark green*) TDP-43-derived fluorescence, represented as a percentage relative to the nuclear fluorescence detected after transfection with vehicle. Experimental errors are S.E. The single (*), double (**), and triple (***) asterisks refer to *p* values lower than 0.05, 0.01, and 0.001, respectively, relative to nuclear or cytoplasmic TDP-43-derived fluorescence of cells transfected with vehicle.

Results

Overexpression of Human TDP-43 in NSC34 Cells Caused Both Nuclear Depletion and Cytoplasmic Accumulation—We first transfected murine NSC34 cells transiently with different quantities (1–20 μg) of the pCI-neo plasmid expressing human TDP-43. The presence of TDP-43 in the cells was assessed 48 h later, using confocal microscopy and monoclonal anti-TDP-43 antibodies that recognize both endogenous (murine) and exogenous (human) TDP-43. Cells transfected with vehicle showed the expected nuclear localization of TDP-43 (Fig. 1). Cells transfected with moderate quantities of plasmid (1–4 μg)

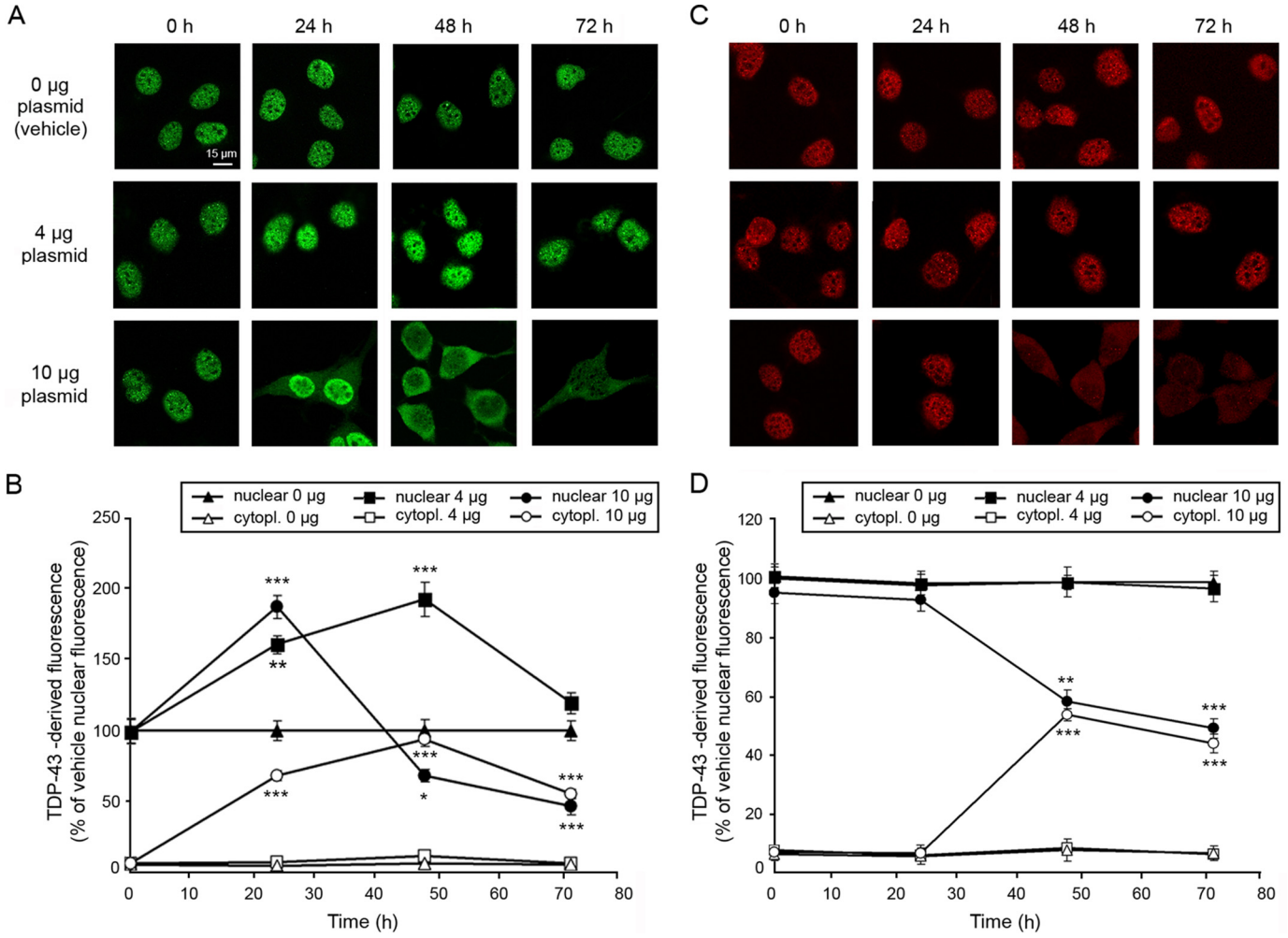

FIGURE 2. *A* and *C*, representative confocal scanning microscope images of murine NSC34 cells transiently transfected with 0, 4, and 10 μg of pCI-neo plasmid expressing human TDP-43, analyzed 0, 24, 48, and 72 h after transfection. The green and red fluorescence indicates TDP-43 detected with antibodies that recognize both endogenous and exogenous protein (*A*) and only endogenous protein (*C*), respectively. *B* and *D*, semi-quantitative analyses of nuclear (*filled symbols*) and cytoplasmic (*empty symbols*) TDP-43-derived fluorescence upon transfection with 0 (*triangles*), 4 (*squares*), and 10 (*circles*) μg of plasmid. The two plots refer to antibodies that recognize both the endogenous and exogenous protein (*B*) and only the endogenous protein (*D*), respectively. Experimental errors are S.E. The single (*), double (**), and triple (***) asterisks refer to *p* values lower than 0.05, 0.01, and 0.001, respectively, relative to nuclear or cytoplasmic TDP-43 derived fluorescence of cells transfected with vehicle.

showed a significant increase in nuclear TDP-43 levels, whereas the cytoplasmic TDP-43-derived fluorescence remained almost unchanged (Fig. 1). By contrast, cells transfected with higher amounts of plasmid (6–10 μg) showed a progressive accumulation of the overexpressed protein in the cytosol along with progressive nuclear clearance (Fig. 1). In particular, transfection of the cells with 10 μg of plasmid led to a significant decrease in nuclear TDP-43 and a large increase in cytoplasmic TDP-43, mimicking the redistribution of TDP-43 from the nucleus to the cytoplasm observed in pathological situations. Moreover, TDP-43 accumulating in the cytosol appeared to be ubiquitinated and phosphorylated at Ser-409/410, as shown by immunofluorescence using antibodies against TDP-43, ubiquitin and phosphorylated TDP-43, again in agreement with the post-translational modifications of TDP-43 observed in pathology (supplemental Fig. S1). Transfection with yet larger amounts of plasmid (15–20 μg) resulted in a progressive reduction of both nuclear and cytoplasmic TDP-43, probably as a consequence of an autoregulation process of the protein (33) and clearance processes mediated by the cells (Fig. 1).

A time-course analysis showed that cells transfected with 4 μg of plasmid underwent a progressive increase in nuclear TDP-43-derived fluorescence at times up to 48 h after transfection, with a significant reduction after 72 h (Fig. 2, *A* and *B*), probably a result of the transient nature of our transfection. By contrast, cytoplasmic TDP-43 levels were not significantly modified (Fig. 2, *A* and *B*). Cells transfected with 10 μg of plasmid showed a significant increase in nuclear TDP-43-derived fluorescence only 24 h after transfection, followed by a significant decrease after 48 h and a dramatic decrease after 72 h (Fig. 2, *A* and *B*). This pattern is likely to be due to the progressive accumulation of TDP-43 in the cytoplasm, which reached a maximum value 48 h after transfection and was able to recruit nuclear TDP-43 (Fig. 2, *A* and *B*). These events were followed by a significant decrease of both nuclear and cytoplasmic TDP-43 levels 72 h after transfection (Fig. 2, *A* and *B*), again probably due to the transient nature of our transfection.

We also monitored the levels of endogenous TDP-43 in the same experiments, using polyclonal antibodies that specifically recognize murine TDP-43. The cross-reactivity of the anti-mu-

rine TDP-43 antibodies with human TDP-43 was excluded (supplemental Fig. S2). Cells transfected with 4 μg of plasmid showed that endogenous TDP-43 remained unmodified and that translocation of endogenous TDP-43 to the cytoplasm had not taken place (Fig. 2, *C* and *D*). This result indicates that the levels of nuclear endogenous TDP-43 did not change with time following overexpression of exogenous TDP-43, and that the time-dependent change of the total TDP-43 observed in the nucleus can be attributed to the transient overexpression of exogenous TDP-43. In contrast, cells transfected with 10 μg of plasmid showed a time-dependent translocation of endogenous TDP-43 from the nucleus to the cytoplasm (Fig. 2, *C* and *D*). This result indicates that there is sequestration of endogenous nuclear TDP-43 by the cytoplasmic exogenous protein, which also accumulates in the cytoplasm under these conditions of transfection.

We next assessed the viability of the NSC34 cells expressing exogenous TDP-43 for 48 h by measuring their ability to reduce MTT (Fig. 3*A*) and to activate caspase-3 (Fig. 3, *B* and *C*). These experiments showed that TDP-43 overexpression generated toxicity, the degree of which increased with the quantities of transfected plasmid. Toxicity was significant following transfection with 4 μg of plasmid for 48 h, *i.e.* under conditions that were accompanied by nuclear TDP-43 accumulation but without significant cytoplasmic accumulation, indicating that an increase in the levels of nuclear TDP-43 is deleterious to the cells (Fig. 3). The toxicity was significantly higher with 10 μg of plasmid, where both nuclear depletion and cytoplasmic accumulation of TDP-43 were evident, indicating that the combination of these events is very highly deleterious to the cells (Fig. 3). Such toxicity could result either from a gain-of-function (GOF) of the accumulated cytoplasmic protein, a loss-of-function (LOF) of the nuclear protein, or both.

Loss of Functional TDP-43 by siRNA Results in Significant Toxicity in NSC34 Cells—To cause nuclear depletion and cytosolic accumulation of TDP-43 separately and independently of each other, and assess their corresponding effects on the cells, we used two strategies: knockdown of endogenous TDP-43 and cell transfection with pre-formed TDP-43 aggregates. We achieved knockdown of endogenous TDP-43 in NSC34 cells by using siRNA, as described in "Experimental Procedures." Confocal microscopy images of cells transfected with vehicle or control siRNA, the latter consisting of a pool of 4 non-targeting siRNAs, did not show any changes in the levels of nuclear or cytosolic TDP-43-derived fluorescence over a period of 72 h (Fig. 4, *A* and *B*). By contrast, cells transfected with siRNA specific for TDP-43 showed a highly significant time-dependent reduction of nuclear TDP-43-derived fluorescence, in the absence of any detectable cytosolic fluorescence (Fig. 4, *A* and *B*). Since we achieved different levels of TDP-43 mRNA silencing by varying the time of incubation after siRNA transfection, for this and following analyses we varied this parameter, while maintaining unaltered the quantity of siRNA used in our transfection.

We also assessed the functionality of nuclear TDP-43 by monitoring its regulation of the splicing activity of the mRNA transcribed from the mouse sortilin 1 (Sort1) gene, as previously described (34). Cells transfected with vehicle and control siRNA showed, after 72 h, an intense band at 250 bp and a weak band at 350 bp, indicating inhibition of the inclusion of the sortilin exon cassette (termed Ex17b) in the Sort1 mRNA and

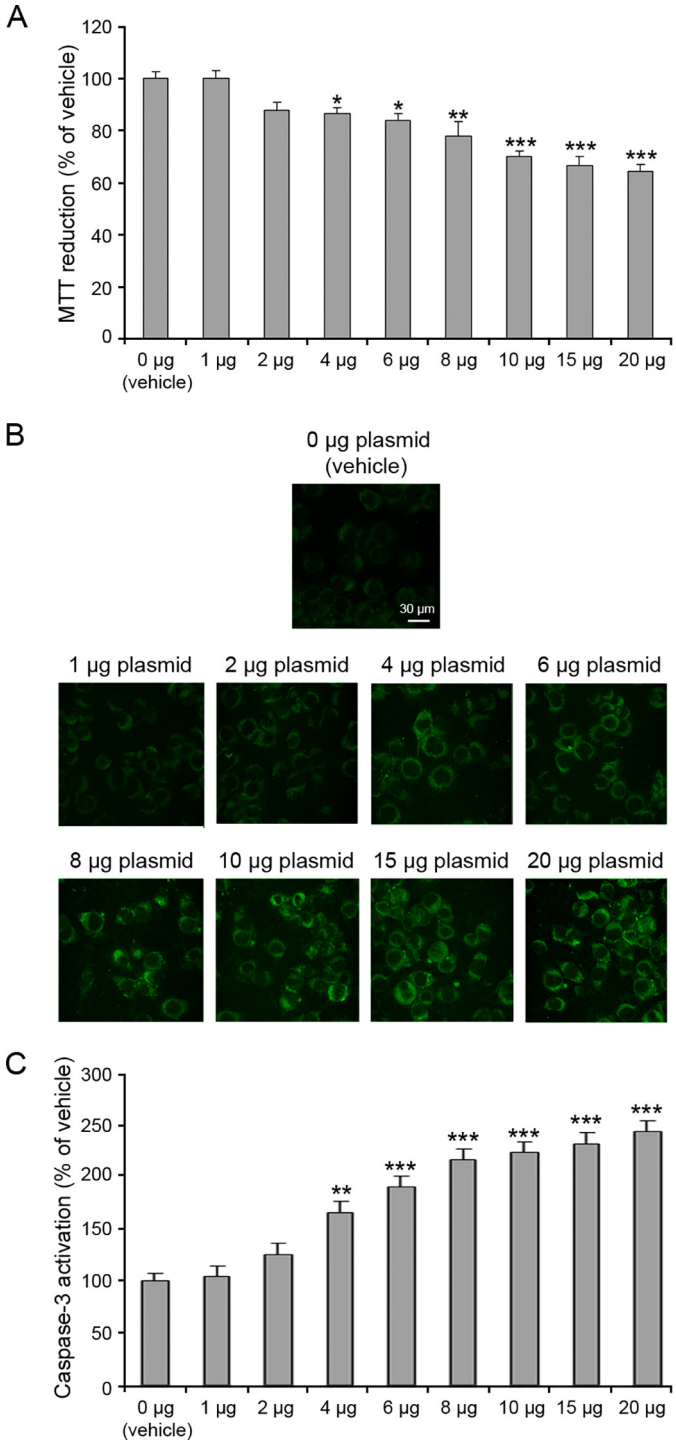

FIGURE 3. *A*, MTT reduction of NSC34 cells 48 h following transfection with different quantities (0–20 μg) of pCI-neo plasmid expressing human TDP-43. *B*, representative confocal microscope images showing caspase-3 activation in NSC34 cells, assessed using the fluorescent probe FAM-FLICA™ caspases 3 and 7. The images were acquired 48 h following transfection with different quantities (0–20 μg) of pCI-neo plasmid expressing human TDP-43. *C*, semi-quantitative analysis of the green fluorescence arising from caspase-3 activation. Experimental errors are S.E. The single (*), double (**), and triple (***) asterisks refer to *p* values lower than 0.05, 0.01, and 0.001, respectively, relative to cells transfected with vehicle.

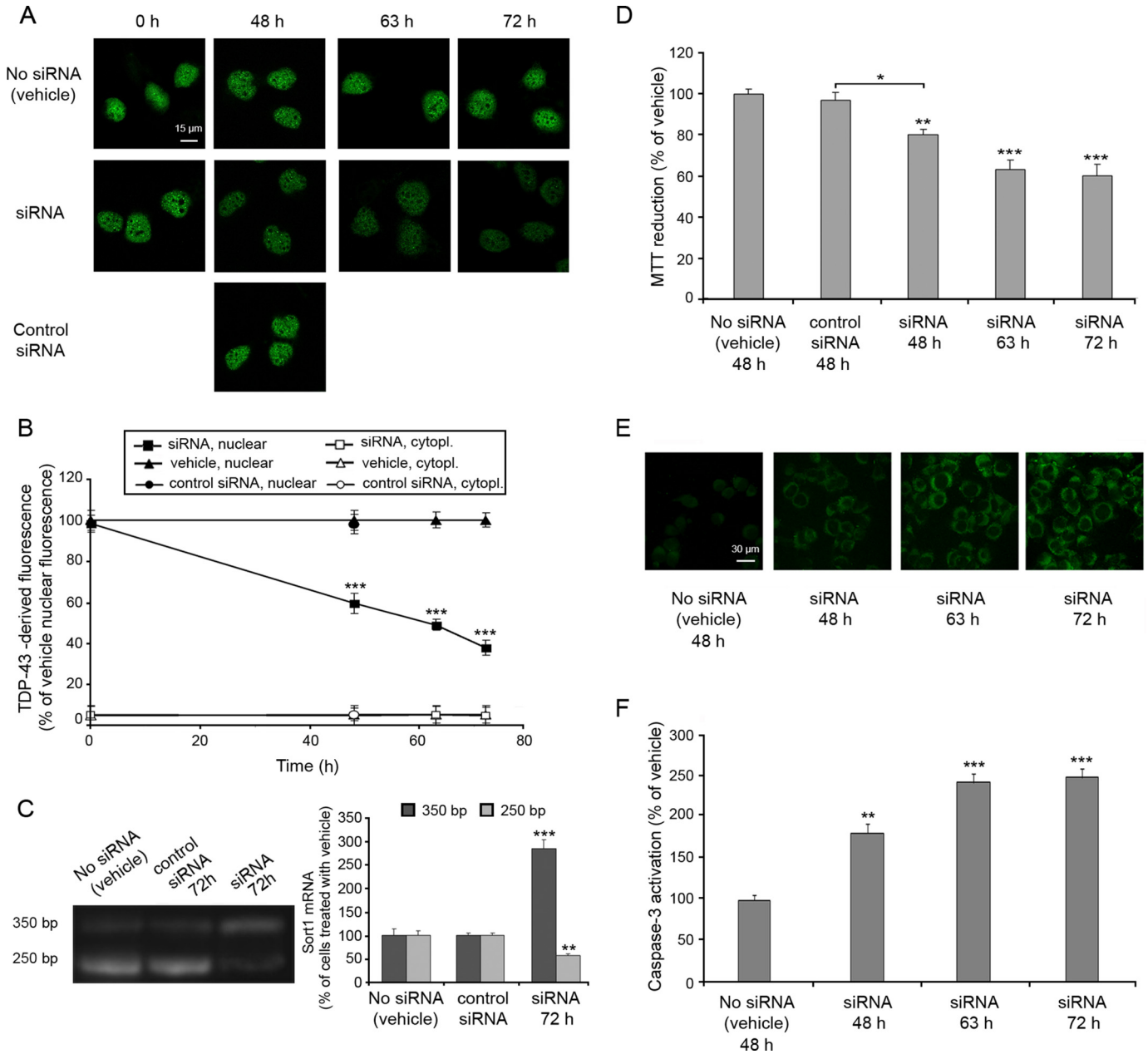

FIGURE 4. *A*, representative confocal scanning microscope images of NSC34 cells transfected with vehicle, 25 nM siRNA and 25 nM control siRNA and analyzed 0, 48, 63, and 72 h after transfection. The *green* fluorescence indicates TDP-43 detected with immunofluorescence. *B*, semi-quantitative analysis of nuclear (*filled symbols*) and cytoplasmic (*empty symbols*) TDP-43-derived fluorescence upon transfection with vehicle (*triangles*), siRNA (*squares*), and control siRNA (*circles*). *C*, splicing analysis of the mouse sortilin 1 (*Sort1*) gene upon TDP-43 silencing and corresponding densitometric analysis in NSC34 cells. The inclusion of the sortilin exon cassette (*Ex17b*) is generated upon TDP-43 down-regulation resulting in a 350-bp band. NSC34 cells were transfected with vehicle, 25 nM control siRNA, and 25 nM siRNA and analyzed after 72 h. *D*, MTT reduction of NSC34 cells transfected with siRNA and analyzed 0, 48, 63, and 72 h after transfection. *E*, representative confocal microscope images showing caspase-3 activation in NSC34 cells, assessed using the fluorescent probe FAM-FLICA™ caspases 3 and 7. The images were acquired at the indicated times, following transfection with vehicle or 25 nM siRNA. *F*, semi-quantitative analysis of the green fluorescence arising from caspase-3 activation. Experimental errors are S.E. The double (**) and triple (***) asterisks refer to *p* values lower than 0.01 and 0.001, respectively, relative to cells transfected with vehicle.

the presence of a functional TDP-43 (Fig. 4*C*). By contrast, cells transfected with siRNA specific for TDP-43 showed, after 72 h, a weaker band at 250 bp and a more intense band at 350 bp, significantly different from those observed with vehicle or control siRNA, as assessed by densitometric analysis of RT-PCR (Fig. 4*C*). This result indicates that the Ex17b exon cassette had been largely included in the mRNA and the function of TDP-43 as a regulator of the Sort1 mRNA splicing was partially impaired (Fig. 4*C*).

Transfection with control siRNA was found to be innocuous to the cells, whereas transfection with TDP-43-specific siRNA induced significant toxicity, which increased with time, as detected with the MTT reduction assay and the measurement of caspase-3 activation (Fig. 4, *D*–*F*). These data suggest that the loss of nuclear, functional TDP-43 is intrinsically toxic and plays an important role in the cytotoxicity associated with TDP-43 pathology, independently of the accumulation of cytoplasmic TDP-43.

Internalization of TDP-43 IBs Generated a Significant Toxicity in NSC34 Cells—To assess the contribution of cytoplasmic TDP-43 inclusions on cellular toxicity, we used bacterial inclusion bodies (IBs) purified from *Escherichia coli* cells after overexpression of human TDP-43 (TDP-43 IBs), as well as IBs purified from *E. coli* cells after overexpression of the same plasmid devoid of the TDP-43 gene (control IBs). We first assessed the content of the TDP-43 IBs formed in *E. coli*, and TDP-43 was detected only in the pellet (P) fraction after cell lysis, indicating that it had aggregated and become located in the IBs after overexpression (supplemental Fig. S3, *A* and *B*). Following purification of the IBs from *E. coli* cell lysates, TDP-43 was again detected only in the P fraction, indicating that it had maintained its aggregated state until the end of the IB purification procedure (supplemental Fig. S3, *A* and *B*). This analysis also showed that TDP-43 IBs contained 30% TDP-43 and 70% of other proteins (supplemental Fig. S3*B*); we therefore used concentrations of TDP-43 IBs that were 30% higher than control IBs so that the two sets of IBs contained the same quantities of non-TDP-43 proteins and differed only in the presence, in the first case, of TDP-43 aggregates. Using this approach, it was possible to evaluate the effects of TDP-43 aggregates within the IBs relative to other aggregated proteins present in IBs by analyzing the differences between control IBs and TDP-43 IBs.

To allow the cellular internalization of purified TDP-43 IBs and control IBs into NSC34 cells we used reagents containing cationic amphiphilic molecules. NSC34 cells transfected with vehicle or 16 μg/ml of control IBs showed the presence of endogenous nuclear TDP-43, in the absence of any accumulation in the cytoplasm (Fig. 5, *A* and *B*). In contrast, cells transfected with TDP-43 IBs showed cytoplasmic TDP-43 accumulation, which increased with the IB concentration, without any significant modification of endogenous nuclear TDP-43 (Fig. 5, *A* and *B*). Antibodies specific for murine TDP-43 confirmed that the newly accumulated cytoplasmic TDP-43 was entirely exogenous (human) and that the levels of endogenous nuclear TDP-43 (murine) were unchanged following TDP-43 IB transfection (Fig. 5*C*). We also examined the splicing of the Sort1 mRNA; cells transfected with vehicle, 4 μg/ml of control IBs and 5.7 μg/ml of TDP-43 IBs, all showed an intense band at 250 bp and a weak band at 350 bp, indicating that the Ex17b sequence had not been included in the Sort1 mRNA and therefore that the endogenous nuclear TDP-43 maintained its function as a regulator of the Sort1 mRNA splicing after IB internalization (Fig. 5*D*).

To assess the aggregation state of the exogenous TDP-43, newly inserted in the cytosol of NSC34 cells using TDP-43 IBs, we purified the cytoplasmic fraction of the cells transfected with 5.7 μg/ml of TDP-43 IBs, separated the soluble and insoluble fractions by centrifugation and analyzed the resulting supernatant (SN) and pellet (P) fractions using Western blotting and anti-TDP-43 antibodies. The exogenous TDP-43 was detected only in the P fraction, indicating that it maintained its aggregated state after cellular internalization (supplemental Fig. S3*C*). Moreover, the newly inserted, cytosolic TDP-43 protein appeared to be ubiquitinated and, at least in part, phosphorylated, as shown by immunofluorescence, mimicking the post-translational modifications observed in pathological situations (supplemental Fig. S4, *A* and *B*). The phosphorylation of TDP-43 IBs was also assessed by Western blotting and anti-TDP-43 phosphorylation sites 409/410 antibodies (supplemental Fig. S4*C*).

We next analyzed the viability of NSC34 cells treated with 1.425–22.8 μg/ml of TDP-43 IBs and with 16.0 μg/ml of control IBs, the latter corresponding to the highest concentration of TDP-43 IBs (30% lower). Cells treated with control IBs showed a low level of cytotoxicity, attributable to the aggregated protein present in the IBs (Fig. 5, *E*–*G*). Cells treated with TDP-43 IBs showed a much higher cytotoxicity, which increased with IB concentration (Fig. 5, *E*–*G*). Since 16 μg/ml of control IBs and 22.8 TDP-43 IBs differed only in the presence of TDP-43, the higher toxicity observed with both assays for TDP-43 IBs relative to control IBs can be attributed to the aggregated TDP-43 present in the IBs. These results suggest that the accumulation of TDP-43 aggregates in the cytoplasm intrinsically induces cellular toxicity and is therefore likely to play an important role in the cytotoxicity associated with TDP-43 pathology, independently of TDP-43 nuclear depletion.

Quantification of GOF and LOF Contributions to Toxicity in NSC34 Cells—To assess further the correlation between nuclear levels of TDP-43 and cytotoxicity we took into account the conditions of both TDP-43 overexpression with the pCI-neo plasmid and TDP-43 silencing with siRNA, in which nuclear TDP-43 levels changed without any significant modification of those in the cytoplasm. To this aim, we analyzed the MTT results of NSC34 cells transfected with moderate amounts of plasmid (1, 2, 4 μg) and with siRNA at different times (48, 63, 72 h). The resulting correlation between MTT reduction and nuclear TDP-43 derived fluorescence was found to fit well to a second order polynomial function, *i.e.* to a parabolic function (Fig. 6*A*). Both increases and decreases of nuclear TDP-43 levels, relative to physiological levels, were found to cause a reduction of cell viability (Fig. 6*A*). We repeated the analysis using measurements of caspase-3 activation as a probe of NSC34 cell toxicity and obtained a clearly similar correlation (Fig. 6*B*).

To assess the relationship between cytoplasmic levels of TDP-43 and cytotoxicity we considered both the conditions of TDP-43 overexpression and TDP-43 IB internalization in which cytoplasmic TDP-43 levels changed without any significant decrease of those in the nucleus. To this end, we considered the MTT results of NSC34 cells transfected with 8 μg of plasmid and with control IBs and TDP-43 IBs (1.425–22.8 μg/ml). A plot of MTT reduction *versus* cytoplasmic TDP-43 derived fluorescence revealed that an increase in cytoplasmic TDP-43 levels correlates strongly with a reduction of cell viability (Fig. 6*C*). The resulting correlation was not only highly significant, but appeared to be approximately linear (Fig. 6*C*). We obtained an even more significant correlation using measurements of caspase-3 activation as a probe of NSC34 cell toxicity (Fig. 6*D*).

Using the equations of best fit for the two correlations of Fig. 6, *A* and *B*, we determined the decrease in MTT reduction and the increase in caspase-3 activation for a 50% loss of nuclear TDP-43 relative to the nuclear TDP-43 estimated after transfection with vehicle. Similarly, using the equations of best fit for

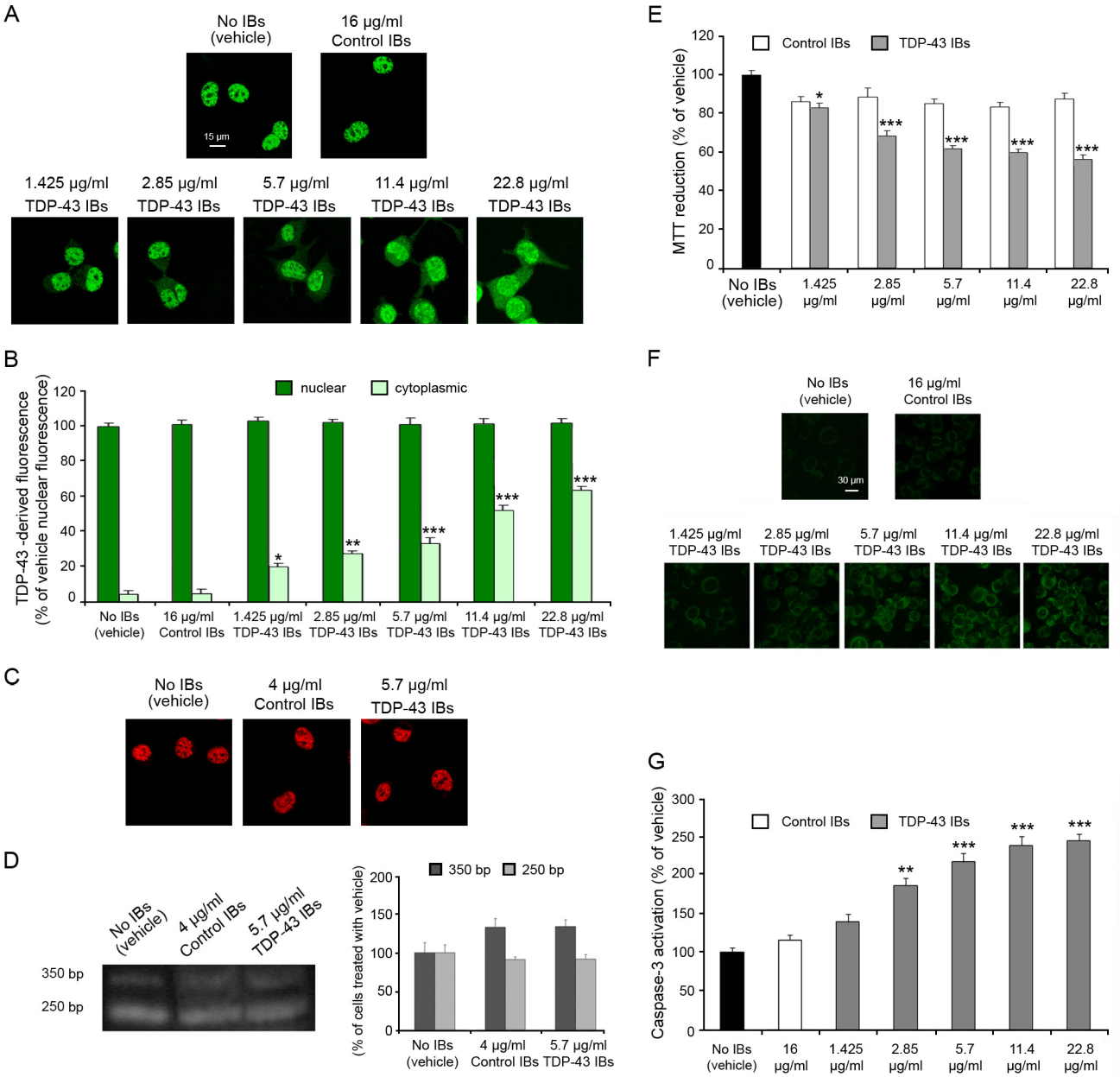

FIGURE 5. *A*, representative confocal scanning microscope images of NSC34 cells transfected with vehicle, 16 μg/ml of control IBs, and different concentrations of TDP-43 IBs and analyzed after transfection. The *green* fluorescence indicates total TDP-43 (human and murine) detected with immunofluorescence. *B*, semi-quantitative analysis of nuclear (*green*) and cytoplasmic (*pale green*) TDP-43-derived fluorescence upon transfection. All data are percentages relative to nuclear fluorescence after transfection with vehicle. The single (*), double (**), and triple (***) asterisks refer to *p* values lower than 0.05, 0.01, and 0.001, respectively, relative to nuclear or cytoplasmic TDP-43-derived fluorescence of cells transfected with vehicle. *C*, representative confocal scanning microscope images of NSC34 cells transfected with vehicle, 4 μg/ml of control IBs and 5.7 μg/ml of TDP-43 IBs and analyzed after transfection with anti-murine TDP-43 antibodies. The red fluorescence indicates murine endogenous TDP-43 detected with immunofluorescence. *D*, splicing analysis of the mouse Sort1 gene upon transfection of NSC34 cells with vehicle, 4 μg/ml of control IBs, and 5.7 μg/ml of TDP-43 IBs and corresponding densitometric analysis. Further details as in Fig. 4*C*. *E*, MTT reduction of NSC34 cells transfected with different concentrations of control IBs and TDP-43 IBs and analyzed after 24 h. The indicated IBs concentrations refer to TDP-43 IBs, which exceed by 30% the corresponding values of control IBs (see the text for the explanation). *F*, representative confocal microscope images of NSC34 cells showing caspase-3 activation, assessed using the fluorescent probe FAM-FLICA™ caspases 3 and 7, 24 h following transfection with the indicated concentrations of control IBs and TDP-43 IBs. *G*, semi-quantitative analysis of the green fluorescence arising from caspase-3 activation. Experimental errors are S.E. The single (*), double (**), and triple (***) asterisks refer to *p* values lower than 0.05, 0.01, and 0.001, respectively, relative to cells transfected with vehicle.

the two correlations of Fig. 6, *C* and *D*, we determined the decrease in MTT reduction and the increase in caspase-3 activation for a 50% accumulation of cytoplasmic TDP-43 relative to the nuclear TDP-43 estimated after transfection with vehicle. This calculation was carried out by interpolating the values of MTT reduction and caspase-3 activation on the *y* axis corresponding to a nuclear TDP-43-derived fluorescence of 50% on the *x* axis (Fig. 6, *A* and *B*) or to a cytoplasmic TDP-43-derived fluorescence of 50% on the *x* axis (Fig. 6, *C* and *D*). The values obtained at 50% of vehicle nuclear TDP-43 allow to compare similar levels of toxicity when the same levels of TDP-43 are depleted form the nucleus (Fig. 6, *A* and *B*) or present in the cytoplasm (Fig. 6, *C* and *D*). To allow the comparison between different parameters of toxicity, the values of caspase-3 activa-

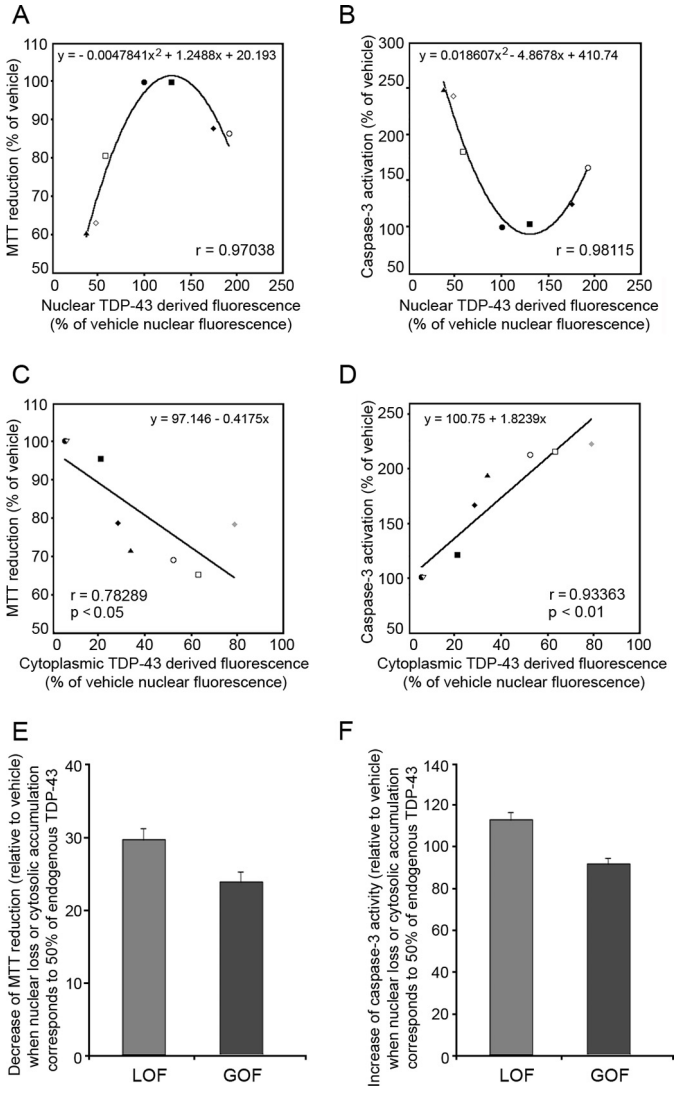

FIGURE 6. *A* and *B*, MTT reduction (*A*) and caspase-3 activation (*B*) *versus* nuclear TDP-43 levels in NSC34 cells transfected with plasmid (1–4 μg) and analyzed after 48 h or with 25 nM siRNA and analyzed after 48–72 h. Data points refer to vehicle (●), 1 μg plasmid (■), 2 μg plasmid (◆), 4 μg plasmid (○), siRNA 48 h (□), siRNA 63 h (◇), and siRNA 72 h (▲). The *solid lines* represent the lines of best fit obtained using a second-order polynomial function, which are also numerically reported in the figures. *C* and *D*, MTT reduction (*C*) and caspase-3 activation (*D*) *versus* cytoplasmic TDP-43 levels in NSC34 cells transfected with control IBs (16 μg/ml) and TDP-43 IBs (1.425–22.8 μg/ml) and analyzed after transfection or 8 μg of plasmid and analyzed 48 h after transfection. Data points refer to control IBs (●), 1.425 μg/ml TDP-43 IBs (■), 2.85 μg/ml TDP-43 IBs (black ◆), 5.7 μg/ml TDP-43 IBs (▲), 11.4 μg/ml TDP-43 IBs (○), 22.8 μg/ml TDP-43 (□), vehicle (▽) and 8 μg plasmid (grey ◆). The *solid lines* represent the straight lines of best fit, which are also numerically reported in the figures. *E* and *F*, decrease of MTT reduction (*E*) and increase of caspase-3 activation (*F*) relative to transfection with vehicle when nuclear loss (*light bars*) or cytosolic accumulation (*dark bars*) corresponds to 50% of nuclear endogenous TDP-43, as determined with transfection with vehicle.

tion were calculated as increase percentages relative to basal levels (for example, values of 213% and 191% were found in Fig. 6, *B* and *D*, respectively, for 50% nuclear depletion or cytosolic enrichment, implying increases of 113% and 91% relative to basal levels, respectively).

This analysis enabled the quantification of the degree of cytotoxicity of NSC34 cells resulting from the loss of nuclear TDP-43 (LOF) and from the gain of aggregated TDP-43 in the cytoplasm (GOF) in similar quantities (Fig. 6, *E* and *F*). Using MTT reduction as a probe of toxicity (Fig. 6, *A* and *C*) we obtained similar values for each function, *i.e.* decreases of MTT reduction of 29.5 ± (1.9)% and 23.7 (±1.6)% at 50% nuclear depletion or cytoplasmic enrichment, respectively (Fig. 6*E*), corresponding to 55.4 (±3.5)% and 44.6 (±3.0)% of the total observed toxicity, summing up both LOF and GOF contributions. Using caspase-3 activation as a probe of toxicity (Fig. 6, *B* and *D*) we again obtained similar values, *i.e.* increases of caspase-3 activity of 113.8 (±4.2)% and 91.9 (±4.0)% at 50% nuclear depletion or cytoplasmic enrichment, respectively (Fig. 6*F*), corresponding to 55.3 (±2.0)% and 44.7 (±2.0)% of the total observed toxicity, summing up both LOF and GOF contributions. These data allow us to conclude that the GOF and LOF mechanisms contribute to ~45% and 55%, respectively, for the NSC34 cell system used here, using both readouts of cell toxicity.

All the data presented in this work, and particularly the correlations and analyses presented in Fig. 6, are based on the levels of nuclear and cytoplasmic TDP-43 measured with confocal microscopy and anti-TDP-43 antibodies. The TDP-43 levels were also, however, quantified using a Western blot analysis of the nuclear and cytoplasmic fractions for NSC34 cells transfected with representative amounts of the pCI-neo plasmid, siRNA or TDP-43 IBs and anti-TDP-43 antibodies. The TDP-43 levels measured with the Western blot technique in the nucleus and cytosol following the various treatments were found to agree clearly with the corresponding values obtained with confocal microscopy (supplemental Fig. S5).

Finally, all the experiments presented in this work were carried out on NSC34 cells. To extend the analysis to a different cell type we repeated some of key experiments with siRNA and TDP-43 IBs on murine neuroblastoma N2a cells (supplemental Figs. S6 and S7). We found that both a loss of nuclear TDP-43 in the absence of cytoplasmic accumulation (supplemental Fig. S6) and accumulation of TDP-43 inclusions in the absence of nuclear TDP-43 depletion (supplemental Fig. S7) lead to levels of toxicity similar to those observed in NSC34 cells under corresponding conditions, confirming that both LOF and GOF mechanisms were similarly important in this cell type.

Discussion

Taken together, the data reported in this manuscript show clearly that both nuclear depletion of soluble and functional TDP-43 and accumulation of the same protein in the form of cytoplasmic inclusions contribute to the deleterious effects associated with the typical TDP-43 pathology observed in neurons and motor neurons of individuals suffering from ALS and FTLD-U. Moreover, the relative contributions of these two effects appear to be clearly similar, *i.e.* ~55% and 45%, respectively, independently of the used cell line (either NSC34 or N2a), of the readout of cell toxicity (either MTT reduction or caspase-3 activity measurements), of the method used to quantify TDP-43 levels (either confocal microscopy coupled to immunofluorescence or Western blotting analysis). This conclusion reconciles the two apparently opposing theories that have been advanced to explain the origins of ALS and FTLD-U as either LOF or GOF diseases, by showing that these fatal and highly debilitating disorders can arise from a combination of

the two contributions that are synergic, and together exacerbate the effects of each on the pathological states associated with TDP-43.

This conclusion provides a rational explanation of the fact that many mutations associated with familial ALS or FTLD-U are located within genes whose protein products are associated with RNA maturation, such as ANG (35), SETX (36), HNRNPA1 (37), TARDBP (38), and FUS (39), while many other mutations involve proteins that aggregate into intracellular inclusions, such as TARDBP (38), FUS (39), SOD1 (40), and C9ORF72 (41), or are involved in the clearance of misfolded proteins via the ubiquitin-proteasome system or autophagy, such as UBQLN2 (42), VCP (43), CHMP2B (44), and OPTN (45).

In summary, therefore, these data provide a unifying description of the pathology of ALS and FTLD-U. In addition, they have profound implications for the design of therapeutic strategies aimed at intervening in the complex cascade of molecular events that constitute ALS and FTLD-U pathogenesis, suggesting that, to be fully effective, such strategies will need to be based on the avoidance of both nuclear clearance and cytoplasmic aggregation of TDP-43.

Experimental Procedures

Cell Cultures—Murine NSC34 and N2a cell lines were cultured as described in supplementary methods.

Transient Transfection—Overexpression of TDP-43 was carried out using the pCI-neo plasmid expressing human TDP-43 (kindly provided by E. Buratti, Italy) as previously reported (13). NSC34 cells were plated in 6-well plates containing coverslips at 150,000 cells/well density. 24 h after plating, the cells were washed with PBS and transfected using Lipofectamine 3000 (Life Technologies), according to the manufacturer's instructions, with different quantities of plasmid (1, 2, 4, 6, 8, 10, 15, and 20 μg), 7 μl of Lipofectamine, 10 μl of transferrin 5 mg/liter, and 5 μl of P3000 reagent in DMEM for 3 h in a 5% CO_2 humidified atmosphere at 37 °C. The cells were also transfected with vehicle (transfection mix without plasmid). 3 h after transfection the DMEM was replaced with fresh complete medium, the cells were incubated for 48 h and then the confocal microscopy experiments were performed. In a set of experiments NSC34 cells were transfected with 4 and 10 μg of plasmid and analyzed after different lengths of time (0, 24, 48, and 72 h) for a time-course analysis.

Transient transfection of pCI-neo plasmid expressing human TDP-43 was also performed on NSC34 cells plated in 96-well plates at 15,000 cells/well density with different quantities of plasmid (0.1, 0.2, 0.4, 0.6, 0.8, 1, 1.5, and 2 μg), 0.7 μl of Lipofectamine, 1 μl of transferrin 5 mg/liter and 0.5 μl of P3000 reagent. 48 h after transfection, the MTT reduction assay was carried out (see below).

RNA Interference—NSC34 cells were plated in 6-well plates containing coverslips at 150,000 cells/well density. 24 h after plating, the cells were washed with PBS and transfected using ON-TARGETplus Mouse Tardbp siRNA SMARTpool (GE Dharmacon, Lafayette, CO), according to the manufacturer's instructions, with 25 nM small-interfering RNA (siRNA), 7 μl of Lipofectamine, 10 μl of 5 mg/liter transferrin in DMEM for 3 h in a 5% CO_2 humidified atmosphere at 37 °C. The cells were also transfected with vehicle (transfection mix without siRNA), and also with control siRNA, consisting of a pool of 4 non-targeting siRNAs. 3 h after transfection the DMEM was replaced with fresh complete medium, the cells were incubated for different lengths of time (48, 63, and 72 h) for a time-course analysis, prior to analysis with confocal microscopy.

RNA interference of TDP-43 was also performed on NSC34 cells plated in 96-well plates at 15,000 cells/well density with 25 nM siRNA, 0.7 μl of Lipofectamine, and 1 μl of 5 mg/liter transferrin. After different lengths of time (48, 63, and 72 h), the MTT reduction assay was carried out (see below).

RNA interference of TDP-43 was also performed on N2a cells plated in 6-well plates containing coverslips at 30,000 cells/well density for confocal microscopy and in 96-well plates at 5,000 cells/well density for the MTT reduction assay. The cells were transfected with vehicle and 25 nM siRNA, and the RNAi of TDP-43 was analyzed 72 h after cell transfection.

Purification and Cell Internalization of TDP-43 IBs—Human TDP-43 was overexpressed in *E. coli* and the resulting inclusion bodies (TDP-43 IBs) were purified, as previously described (46). NSC34 cells were plated in 6-well plates containing coverslips at 150,000 cells/well density. 24 h after plating, the cells were washed with PBS and transfected using the PULSin protein delivery reagent (Polyplus-transfection, Illkirch, France), according to the manufacturer's instructions, with different concentrations of control IBs (2, 4, 8, and 16 μg/ml) and TDP-43 IBs (1.425, 2.85, 5.7, 11.4, and 22.8 μg/ml), 100 μl of 20 mM Hepes Buffer and 4 μl of PLUSin reagent in cell culture medium without FBS (46). The cells were also transfected with vehicle (transfection mix without IBs). 2 h after transfection the medium without FBS was replaced with fresh complete medium and the confocal microscopy experiments were carried out (see below).

Transfection of IBs was also performed on NSC34 cells plated in 96-well plate at 15,000 cells/well density with different concentrations of control IBs and TDP-43 IBs, 10 μl of 20 mM Hepes Buffer and 0.4 μl of PLUSin reagent. 24 h after transfection, the MTT reduction assay was carried out (see below).

The transfection of IBs was also carried out in N2a cells plated in 6-well plates containing coverslips at 30,000 cells/well density for confocal microscopy and in 96-well plates at 5,000 cells/well density for the MTT reduction assay. The cells were transfected with vehicle, 4 μg/ml of control IBs and 5.7 μg/ml of TDP-43 IBs. IBs internalization was analyzed after cell transfection, whereas the cell viability was assessed after 24 h, as described above.

Confocal Microscopy Analysis of TDP-43 Levels—NSC34 cells were transfected with 1–20 μg of plasmid, 25 nM siRNA, 1.425–22.8 μg/ml of TDP-43 IBs, or 1–16 μg/ml of control IBs and incubated for different lengths of time, as described above. After washing with PBS, the cells were fixed in 2% (w/v) buffered paraformaldehyde for 10 min at room temperature (~20 °C) and permeabilized with a solution of PBS plus 0.5% (v/v) Triton X-100 and 0.5% bovine serum albumin (BSA) for 5 min at room temperature (~ 20 °C). Then, the cells were incubated for 60 min at 37 °C with 1:500 diluted mouse monoclonal anti-TDP-43 antibodies (Novus Biologicals, Ltd, Cambridge,

UK) in PBS plus 1% of FBS, and for 90 min with 1:1000 diluted Alexa Fluor 488-conjugated anti-mouse secondary antibodies in PBS plus 1% of FBS. In another experimental set, N2a cells were transfected with 25 nM siRNA, 5.7 μg/ml of TDP-43 IBs, or 4 μg/ml of control IBs and analyzed as described above.

The analysis was repeated using antibodies that recognize only the murine protein. NSC34 and N2a cells were transfected with 4 and 10 μg of plasmid, 4 μg/ml of control IBs and 5.7 μg/ml of TDP-43 IBs, and analyzed as described above using 1:500 diluted rabbit polyclonal anti murine TDP-43 antibodies (LSBio, Seattle, WA) and 1:1000 diluted Alexa Fluor 594-conjugated anti-rabbit secondary antibodies.

Cells were analyzed using a Leica TCS SP5 confocal scanning microscope (Leica Microsystems, Mannheim, Germany), equipped with an argon laser source and a Leica Plan Apo 63 × oil immersion objective. A series of optical sections (1024 × 1024 pixels) 1.0 μm in thickness was taken through the cell depth for each sample examined. The confocal microscope was set at optimal acquisition conditions of pinhole diameter, detector gain and laser power, and the settings were maintained constant for each analysis. To quantify the signal intensity, 10–22 cells in three different experiments were analyzed using ImageJ software (NIH, Bethesda, MD) and both cytoplasmic and nuclear fluorescence intensities were expressed as percentages compared with nuclear fluorescence measured after transfection with the vehicle (taken as 100%).

MTT Reduction Assay—The MTT reduction assay was performed on NSC34 cells transfected with vehicle, 1–20 μg of plasmid for 48 h, 25 nM siRNA for different lengths of time (48, 63, and 72 h), 1–16 μg/ml of control IBs and 1.425–22.8 μg/ml of TDP-43 IBs for 24 h, as previously reported (47). Cell viability was expressed as the percentage reduction of MTT in treated cells relative to the cells treated with vehicle (taken as 100%). The MTT test was also assessed on N2a cells transfected with 25 nM siRNA (72 h), 4 μg/ml of control IBs (24 h) and 5.7 μg/ml of TDP-43 IBs (24 h).

Measurement of Caspase-3 Activity—The levels of caspase-3 activity were analyzed on NSC34 and N2a cells treated as described in the previous subsection by using FAMFLICA™ caspases 3&7 solution (caspase 3&7 FLICA kit FAM-DEVD-FMK, Immunochemistry Technologies, LLC, Bloomington, MN) as previously reported (48). To quantify the signal intensity of caspases 3 and 7 solution, 10–22 cells in three different experiments were analyzed using ImageJ software (NIH, Bethesda, MD), and the fluorescence intensities were expressed as percentages compared with cells transfected with vehicle (taken as 100%).

Splicing Analysis—The functionality of nuclear TDP-43 was analyzed by monitoring its regulation of the splicing activity of the mRNA transcribed from the mouse sortilin 1 (Sort1) gene, as previously described (34). The inclusion of the sortilin exon cassette (termed Ex17b) is generated and translated into protein upon TDP-43 down-regulation. NSC34 cells were transfected with vehicle, 25 nM control siRNA, and 25 nM siRNA for 72 h, or with 4 μg/ml control IBs and 5.7 μg/ml TDP-43 IBs. After treatment, RNA was collected by using TRI Reagent (Sigma-Aldrich). cDNA was prepared and subjected to PCR using primers in exons 17 and 19 of mouse Sort1. The relative levels of exon inclusion were visualized on 1.5% agarose gels. A 350-bp and a 250-bp band products were produced. The densitometric analysis was carried out from three different experiments using ImageJ software (NIH, Bethesda, MD).

Statistical Analysis—Data were expressed as means ± S.E. Comparisons between different groups were performed using ANOVA followed by Bonferroni's post-comparison test. A p value lower than 0.05 was considered statistically significant. The single (*), double (**), and triple (***) asterisks refer to p values lower than 0.05, 0.01, and 0.001, respectively.

Author Contributions—F. C. and C. Cecchi designed and supervised the experiments. R.C. and G.F. maintained cell cultures and performed the confocal microscopy experiments, the splicing analysis, and Western blot analysis. C. Capitini purified IBs. F. C., C. Cecchi, C. M. D., and R. C. interpreted the data and wrote the manuscript.

Acknowledgment—We thank Neil Cashman for providing the NSC34 cell line.

References

1. Neumann, M., Sampathu, D. M., Kwong, L. K., Truax, A. C., Micsenyi, M. C., Chou, T. T., Bruce, J., Schuck, T., Grossman, M., Clark, C. M., McCluskey, L. F., Miller, B. L., Masliah, E., Mackenzie, I. R., Feldman, H., *et al.* (2006) Ubiquitinated TDP-43 in frontotemporal lobar degeneration and amyotrophic lateral sclerosis. *Science* **314,** 130–133
2. Mackenzie, I. R., Bigio, E. H., Ince, P. G., Geser, F., Neumann, M., Cairns, N. J., Kwong, L. K., Forman, M. S., Ravits, J., Stewart, H., Eisen, A., McClusky, L., Kretzschmar, H. A., Monoranu, C. M., Highley, J. R., *et al.* (2007) Pathological TDP-43 distinguishes sporadic amyotrophic lateral sclerosis from amyotrophic lateral sclerosis with SOD1 mutations. *Ann. Neurol.* **61,** 427–434
3. Rowland, L. P., and Shneider, N. A. (2001) Amyotrophic lateral sclerosis. *N. Engl. J. Med.* **344,** 1688–1700
4. Wijesekera, L. C., and Leigh, P. N. (2009) Amyotrophic lateral sclerosis. *Orphanet. J. Rare. Dis.* **4,** 3
5. Diehl-Schmid, J., Onur, O. A., Kuhn, J., Gruppe, T., and Drzezga, A. (2014) Imaging frontotemporal lobar degeneration. *Curr. Neurol. Neurosci. Rep.* **14,** 489
6. Ratti, A., and Buratti, E. (2016) Physiological functions and pathobiology of TDP-43 and FUS/TLS proteins. *J. Neurochem.* 10.1111/jnc.13625
7. Baloh, R. H. (2011) TDP-43: the relationship between protein aggregation and neurodegeneration in amyotrophic lateral sclerosis and frontotemporal lobar degeneration. *FEBS J.* **278,** 3539–3549
8. Lee, E. B., Lee, V. M., and Trojanowski, J. Q. (2012) Gains or losses: molecular mechanisms of TDP-43-mediated neurodegeneration. *Nat. Rev. Neurosci.* **13,** 38–50
9. Halliday, G., Bigio, E. H., Cairns, N. J., Neumann, M., Mackenzie, I. R., and Mann, D. M. (2012) Mechanisms of disease in frontotemporal lobar degeneration: gain of function versus loss of function effects. *Acta Neuropathol.* **124,** 373–382
10. Dewey, C. M., Cenik, B., Sephton, C. F., Johnson, B. A., Herz, J., and Yu, G. (2012) TDP-43 aggregation in neurodegeneration: are stress granules the key? *Brain Res.* **1462,** 16–25
11. Xu, Z. S. (2012) Does a loss of TDP-43 function cause neurodegeneration? *Mol. Neurodegener.* **7,** 27
12. Winton, M. J., Igaz, L. M., Wong, M. M., Kwong, L. K., Trojanowski, J. Q., and Lee, V. M. (2008) Disturbance of nuclear and cytoplasmic TAR DNA-binding protein (TDP-43) induces disease-like redistribution, sequestration, and aggregate formation. *J. Biol. Chem.* **283,** 13302–13309
13. Ayala, Y. M., Zago, P., D'Ambrogio, A., Xu, Y. F., Petrucelli, L., Buratti, E., and Baralle, F. E. (2008) Structural determinants of the cellular localization and shuttling of TDP-43. *J. Cell Sci.* **121,** 3778–3785
14. Igaz, L. M., Kwong, L. K., Chen-Plotkin, A., Winton, M. J., Unger, T. L., Xu,

Y., Neumann, M., Trojanowski, J. Q., and Lee, V. M. (2009) Expression of TDP-43 C-terminal fragments in vitro recapitulates pathological features of TDP-43 proteinopathies. *J. Biol. Chem.* **284,** 8516–8524
15. Zhang, Y. J., Xu, Y. F., Cook, C., Gendron, T. F., Roettges, P., Link, C. D., Lin, W. L., Tong, J., Castanedes-Casey, M., Ash, P., Gass, J., Rangachari, V., Buratti, E., Baralle, F., Golde, T. E., *et al.* (2009) Aberrant cleavage of TDP-43 enhances aggregation and cellular toxicity. *Proc. Natl. Acad. Sci. U.S.A.* **106,** 7607–7612
16. Nonaka, T., Kametani, F., Arai, T., Akiyama, H., and Hasegawa, M. (2009) Truncation and pathogenic mutations facilitate the formation of intracellular aggregates of TDP-43. *Hum. Mol. Genet.* **18,** 3353–3364
17. Kabashi, E., Lin, L., Tradewell, M. L., Dion, P. A., Bercier, V., Bourgouin, P., Rochefort, D., Bel Hadj, S., Durham, H. D., Vande Velde, C., Rouleau, G. A., and Drapeau, P. (2010) Gain and loss of function of ALS-related mutations of TARDBP (TDP-43) cause motor deficits in vivo. *Hum. Mol. Genet.* **19,** 671–683
18. Suzuki, H., Lee, K., and Matsuoka, M. (2011) TDP-43-induced death is associated with altered regulation of BIM and Bcl-xL and attenuated by caspase-mediated TDP-43 cleavage. *J. Biol. Chem.* **286,** 13171–13183
19. Wu, L. S., Cheng, W. C., and Shen, C. K. (2013) Similar dose-dependence of motor neuron cell death caused by wild type human TDP-43 and mutants with ALS-associated amino acid substitutions. *J. Biomed. Sci.* **20,** 33
20. Liu, Y. J., Ju, T. C., Chen, H. M., Jang, Y. S., Lee, L. M., Lai, H. L., Tai, H. C., Fang, J. M., Lin, Y. L., Tu, P. H., and Chern, Y. (2015) Activation of AMP-activated protein kinase α1 mediates mislocalization of TDP-43 in amyotrophic lateral sclerosis. *Hum. Mol. Genet.* **24,** 787–801
21. Iguchi, Y., Katsuno, M., Niwa, J., Yamada, S., Sone, J., Waza, M., Adachi, H., Tanaka, F., Nagata, K., Arimura, N., Watanabe, T., Kaibuchi, K., and Sobue, G. (2009) TDP-43 depletion induces neuronal cell damage through dysregulation of Rho family GTPases. *J. Biol. Chem.* **284,** 22059–22066
22. Wegorzewska, I., Bell, S., Cairns, N. J., Miller, T. M., and Baloh, R. H. (2009) TDP-43 mutant transgenic mice develop features of ALS and frontotemporal lobar degeneration. *Proc. Natl. Acad. Sci. U.S.A.* **106,** 18809–18814
23. Wils, H., Kleinberger, G., Janssens, J., Pereson, S., Joris, G., Cuijt, I., Smits, V., Ceuterick-de Groote, C., Van Broeckhoven, C., and Kumar-Singh, S. (2010) TDP-43 transgenic mice develop spastic paralysis and neuronal inclusions characteristic of ALS and frontotemporal lobar degeneration. *Proc. Natl. Acad. Sci. U.S.A.* **107,** 3858–3863
24. Tsai, K. J., Yang, C. H., Fang, Y. H., Cho, K. H., Chien, W. L., Wang, W. T., Wu, T. W., Lin, C. P., Fu, W. M., and Shen, C. K. (2010) Elevated expression of TDP-43 in the forebrain of mice is sufficient to cause neurological and pathological phenotypes mimicking FTLD-U. *J. Exp. Med.* **207,** 1661–1673
25. Shan, X., Chiang, P. M., Price, D. L., and Wong, P. C. (2010) Altered distributions of Gemini of coiled bodies and mitochondria in motor neurons of TDP-43 transgenic mice. *Proc. Natl. Acad. Sci. U.S.A.* **107,** 16325–16330
26. Igaz, L. M., Kwong, L. K., Lee, E. B., Chen-Plotkin, A., Swanson, E., Unger, T., Malunda, J., Xu, Y., Winton, M. J., Trojanowski, J. Q., and Lee, V. M. (2011) Dysregulation of the ALS-associated gene TDP-43 leads to neuronal death and degeneration in mice. *J. Clin. Invest.* **121,** 726–738
27. Tian, T., Huang, C., Tong, J., Yang, M., Zhou, H., and Xia, X. G. (2011) TDP-43 potentiates alpha-synuclein toxicity to dopaminergic neurons in transgenic mice. *Int. J. Biol. Sci.* **7,** 234–243
28. Cannon, A., Yang, B., Knight, J., Farnham, I. M., Zhang, Y., Wuertzer, C. A., D'Alton, S., Lin, W. L., Castanedes-Casey, M., Rousseau, L., Scott, B., Jurasic, M., Howard, J., Yu, X., Bailey, R., *et al.* (2012) Neuronal sensitivity to TDP-43 overexpression is dependent on timing of induction. *Acta Neuropathol.* **123,** 807–823
29. Xu, Y. F., Gendron, T. F., Zhang, Y. J., Lin, W. L., D'Alton, S., Sheng, H., Casey, M. C., Tong, J., Knight, J., Yu, X., Rademakers, R., Boylan, K., Hutton, M., McGowan, E., Dickson, D. W., *et al.* (2010) Wild-type human TDP-43 expression causes TDP-43 phosphorylation, mitochondrial aggregation, motor deficits, and early mortality in transgenic mice. *J. Neurosci.* **30,** 10851–10859
30. Wu, L. S., Cheng, W. C., Hou, S. C., Yan, Y. T., Jiang, S. T., and Shen, C. K. (2010) TDP-43, a neuro-pathosignature factor, is essential for early mouse embryogenesis. *Genesis* **48,** 56–62
31. Sephton, C. F., Good, S. K., Atkin, S., Dewey, C. M., Mayer, P., 3rd, Herz, J., and Yu, G. (2010) TDP-43 is a developmentally regulated protein essential for early embryonic development. *J. Biol. Chem.* **285,** 6826–6834. Erratum in: *J. Biol. Chem.* **285,** 38740
32. Kraemer, B. C., Schuck, T., Wheeler, J. M., Robinson, L. C., Trojanowski, J. Q., Lee, V. M., and Schellenberg, G. D. (2010) Loss of murine TDP-43 disrupts motor function and plays an essential role in embryogenesis. *Acta Neuropathol.* **119,** 409–419
33. Ayala, Y. M., De Conti, L., Avendaño-Vázquez, S. E., Dhir, A., Romano, M., D'Ambrogio, A., Tollervey, J., Ule, J., Baralle, M., Buratti, E., and Baralle, F. E. (2011) TDP-43 regulates its mRNA levels through a negative feedback loop. *EMBO J.* **30,** 277–288
34. Prudencio, M., Jansen-West, K. R., Lee, W. C., Gendron, T. F., Zhang, Y. J., Xu, Y. F., Gass, J., Stuani, C., Stetler, C., Rademakers, R., Dickson, D. W., Buratti, E., and Petrucelli, L. (2012) Misregulation of human sortilin splicing leads to the generation of a nonfunctional progranulin receptor. *Proc. Natl. Acad. Sci. U.S.A.* **109,** 21510–21515
35. Wu, D., Yu, W., Kishikawa, H., Folkerth, R. D., Iafrate, A. J., Shen, Y., Xin, W., Sims, K., and Hu, G. F. (2007) Angiogenin loss-of-function mutations in amyotrophic lateral sclerosis. *Ann. Neurol.* **62,** 609–617
36. Chen, Y. Z., Bennett, C. L., Huynh, H. M., Blair, I. P., Puls, I., Irobi, J., Dierick, I., Abel, A., Kennerson, M. L., Rabin, B. A., Nicholson, G. A., Auer-Grumbach, M., Wagner, K., De Jonghe, P., Griffin, J. W., *et al.* (2004) DNA/RNA helicase gene mutations in a form of juvenile amyotrophic lateral sclerosis (ALS4). *Am. J. Hum. Genet.* **74,** 1128–1135
37. Kim, H. J., Kim, N. C., Wang, Y. D., Scarborough, E. A., Moore, J., Diaz, Z., MacLea, K. S., Freibaum, B., Li, S., Molliex, A., Kanagaraj, A. P., Carter, R., Boylan, K. B., Wojtas, A. M., Rademakers, R., *et al.* (2013) Mutations in prion-like domains in hnRNPA2B1 and hnRNPA1 cause multisystem proteinopathy and ALS. *Nature* **495,** 467–473
38. Sreedharan, J., Blair, I. P., Tripathi, V. B., Hu, X., Vance, C., Rogelj, B., Ackerley, S., Durnall, J. C., Williams, K. L., Buratti, E., Baralle, F., de Belleroche, J., Mitchell, J. D., Leigh, P. N., Al-Chalabi, A., *et al.* (2008) TDP-43 mutations in familial and sporadic amyotrophic lateral sclerosis. *Science* **319,** 1668–1672
39. Vance, C., Rogelj, B., Hortobágyi, T., De Vos, K. J., Nishimura, A. L., Sreedharan, J., Hu, X., Smith, B., Ruddy, D., Wright, P., Ganesalingam, J., Williams, K. L., Tripathi, V., Al-Saraj, S., Al-Chalabi, A., *et al.* (2009) Mutations in FUS, an RNA processing protein, cause familial amyotrophic lateral sclerosis type 6. *Science* **323,** 1208–1211
40. Kato, S., Rogelj, B., Hortobágyi, T., De Vos, K. J., Nishimura, A. L., Sreedharan, J., Hu, X., Smith, B., Ruddy, D., Wright, P., Ganesalingam, J., Williams, K. L., Tripathi, V., Al-Saraj, S., Al-Chalabi, A., *et al.* (2000) New consensus research on neuropathological aspects of familial amyotrophic lateral sclerosis with superoxide dismutase 1 (SOD1) gene mutations: inclusions containing SOD1 in neurons and astrocytes. *Amyotroph. Lateral. Scler. Other Motor Neuron. Disord.* **1,** 163–184
41. Mori, K., Weng, S. M., Arzberger, T., May, S., Rentzsch, K., Kremmer, E., Schmid, B., Kretzschmar, H. A., Cruts, M., Van Broeckhoven, C., Haass, C., and Edbauer, D. (2013) The C9orf72 GGGGCC repeat is translated into aggregating dipeptide-repeat proteins in FTLD/ALS. *Science* **339,** 1335–1338
42. Deng, H. X., Chen, W., Hong, S. T., Boycott, K. M., Gorrie, G. H., Siddique, N., Yang, Y., Fecto, F., Shi, Y., Zhai, H., Jiang, H., Hirano, M., Rampersaud, E., Jansen, G. H., Donkervoort, S., *et al.* (2011) Mutations in UBQLN2 cause dominant X-linked juvenile and adult-onset ALS and ALS/dementia. *Nature* **477,** 211–215
43. Johnson, J. O., Mandrioli, J., Benatar, M., Abramzon, Y., Van Deerlin, V. M., Trojanowski, J. Q., Gibbs, J. R., Brunetti, M., Gronka, S., Wuu, J., Ding, J., McCluskey, L., Martinez-Lage, M., Falcone, D., Hernandez, D. G., *et al.* (2010) Exome sequencing reveals VCP mutations as a cause of familial ALS. *Neuron* **68,** 857–864
44. Parkinson, N., Ince, P. G., Smith, M. O., Highley, R., Skibinski, G., Andersen, P. M., Morrison, K. E., Pall, H. S., Hardiman, O., Collinge, J., Shaw, P. J., Fisher E. M., MRC Proteomics in ALS Study; and FReJA Consortium (2006) ALS phenotypes with mutations in CHMP2B (charged multivesicular body protein 2B). *Neurology* **67,** 1074–1077

45. Maruyama, H., Morino, H., Ito, H., Izumi, Y., Kato, H., Watanabe, Y., Kinoshita, Y., Kamada, M., Nodera, H., Suzuki, H., Komure, O., Matsuura, S., Kobatake, K., Morimoto, N., Abe, K., *et al.* (2010) Mutations of optineurin in amyotrophic lateral sclerosis. *Nature* **465,** 223–226
46. Capitini, C., Conti, S., Perni, M., Guidi, F., Cascella, R., De Poli, A., Penco, A., Relini, A., Cecchi, C., and Chiti, F. (2014) TDP-43 inclusion bodies formed in bacteria are structurally amorphous, non-amyloid and inherently toxic to neuroblastoma cells. *PLoS ONE* **9,** e86720
47. Evangelisti, E., Wright, D., Zampagni, M., Cascella, R., Fiorillo, C., Bagnoli, S., Relini, A., Nichino, D., Scartabelli, T., Nacmias, B., Sorbi, S., and Cecchi, C. (2013) Lipid rafts mediate amyloid-induced calcium dyshomeostasis and oxidative stress in Alzheimer's disease. *Curr. Alzheimer Res.* **10,** 143–153
48. Cascella, R., Conti, S., Mannini, B., Li, X., Buxbaum, J. N., Tiribilli, B., Chiti, F., and Cecchi, C. (2013) Transthyretin suppresses the toxicity of oligomers formed by misfolded proteins in vitro. *Biochim. Biophys. Acta* **1832,** 2302–2314
49. Cashman, N. R., Durham, H. D., Blusztajn, J. K., Oda, K., Tabira, T., Shaw, I. T., Dahrouge, S., and Antel, J. P. (1992) Neuroblastoma x spinal cord (NSC) hybrid cell lines resemble developing motor neurons. *Dev. Dyn.* **194,** 209–221
50. Simeoni, S., Mancini, M. A., Stenoien, D. L., Marcelli, M., Weigel, N. L., Zanisi, M., Martini, L., and Poletti, A. (2000) Motoneuronal cell death is not correlated with aggregate formation of androgen receptors containing an elongated polyglutamine tract. *Hum. Mol. Genet.* **9,** 133–144
51. Cappelli, S., Penco, A., Mannini, B., Cascella, R., Wilson, M. R., Ecroyd, H., Li, X., Buxbaum, J. N., Dobson, C. M., Cecchi, C., Relini, A., Chiti, F. (2016) Effect of molecular chaperones on aberrant protein oligomers *in vitro*: super- versus sub-stoichiometric chaperone concentrations. *Biol. Chem.* **397,** 401–415
52. Rasband, W. S. (1997–2008) ImageJ, US, National Institutes of Health, Bethesda, Maryland. (rsb.info.nih.gov/ij/).
53. Laemmli, U. K. (1970) Cleavage of structural proteins during the assembly of the head of bacteriophage T4. *Nature* **227,** 680–685